

**Fluorescence activation with switchable oxazines**

Journal:	<i>ChemComm</i>
Manuscript ID	CC-FEA-04-2018-003094.R1
Article Type:	Feature Article

SCHOLARONE™  
Manuscripts

# Fluorescence activation with switchable oxazines

Yang Zhang, Sicheng Tang, Ek Raj Thapaliya, Lorenzo Sansalone and Francisco M. Raymo\*

*Laboratory for Molecular Photonics, Department of Chemistry, University of Miami, 1301 Memorial Drive, Coral Gables, FL 33146-0431, United States*

The identification of operating principles to activate fluorescence under the influence of external stimulations is essential to enable the implementation of imaging strategies requiring the spatiotemporal control of emission. In this context, our laboratories designed mechanisms to switch fluorescence with either light or pH based on the unique photochemical and photophysical properties of either photoresponsive or halochromic oxazines respectively. These heterocycles can be connected covalently to fluorescent chromophores and opened with either light or pH to impose a significant bathochromic shift on the main absorption of the emissive appendage. Such a spectral change allows the selective excitation of the resulting species to activate bright fluorescence with infinite contrast and spatiotemporal control. Indeed, these mechanisms for fluorescence activation enable the acquisition of images with subdiffraction resolution, the selective signaling of cancer cells and the monitoring of translocating species in real time. Thus, our structural designs for fluorescence switching under external control can evolve into invaluable probes for the implementation of bioimaging strategies that would be impossible to perform with conventional fluorophores.

## Introduction

Conventional fluorophores emit light in response to illumination at an appropriate excitation wavelength ( $\lambda_{\text{EX}}$ ).<sup>1</sup> Activatable fluorophores instead produce fluorescence only after the application of an external stimulation prior to excitation.<sup>2-7</sup> Generally, either a chemical input or irradiation at a suitable activation wavelength ( $\lambda_{\text{AC}}$ ) converts a nonemissive reactant into an emissive product.

Excitation of the latter at  $\lambda_{\text{Ex}}$  then generates fluorescence. Under these conditions, the interplay of activating stimulation and excitation can be exploited to switch fluorescence on in a defined region of space at a precise interval of time. Such a level of spatiotemporal control on emission permits the implementation of imaging schemes that would be impossible to perform with conventional fluorophores. For example, the activation of fluorescence in response to chemicals overexpressed in the intracellular environment of target cells allows their selective marking with fluorescent probes.<sup>8-11</sup> Alternatively, optical activation can be exploited to generate fluorescent species in a precise location within a given sample of interest and visualize their subsequent translocation across the specimen in real time with the sequential acquisition of images.<sup>12-15</sup> Similarly, reiterative photoactivation and imaging protocols permit also the differentiation of closely-spaced fluorophores in time and the sequential reconstruction of images with subdiffraction resolution.<sup>16-18</sup> In fact, activatable fluorophores are becoming invaluable probes for the selective detection of cells, the monitoring of dynamic events and the visualization of features with nanoscaled dimensions. Indeed, the identification of viable structural designs to activate bright fluorescence with high contrast is crucial for the further development of these promising imaging strategies into practical analytical methods for the biomedical laboratory.

Electronic transitions are responsible for the ability of conventional fluorophores to absorb radiation with wavelengths ranging from the ultraviolet to the near-infrared region of the electromagnetic spectrum.<sup>1</sup> These processes excite the absorbing species from a ground electronic state ( $S_0$ ) to one of the accessible excited electronic states. Internal conversion generally follows excitation to release part of the absorbed energy in the form of heat and populate the first singlet excited state ( $S_1$ ). The excited chromophore then decays from  $S_1$  back to  $S_0$  either nonradiatively, by releasing further thermal energy, or radiatively, by emitting light in the form of fluorescence. The rates of the two decay pathways dictate the emission quantum yield and, when the radiative process is significantly faster than the nonradiative counterpart, most of the absorbed energy is converted into fluorescence. Thus, the ability to regulate the rate of one decay process relative to the other with external control offers the opportunity to tune the fluorescence quantum yield and, possibly, convert a weakly emissive reactant

into a strongly fluorescent product. Indeed, most activatable fluorophores developed so far operate on the basis of this general mechanism.<sup>7</sup> For example, a conventional fluorophore can be connected covalently to a photocleavable quencher. Excitation of the former at  $\lambda_{\text{EX}}$  populates its  $S_1$  state. The presence of the latter, however, promotes the nonradiative decay of  $S_1$  back to  $S_0$  and only negligible fluorescence is produced. Illumination at a  $\lambda_{\text{AC}}$  that can induce the cleavage of the two components away from each other essentially eliminates the influence of the quencher on the excitation dynamics of the fluorophore. As a result, excitation of fluorophore at  $\lambda_{\text{EX}}$  can now be followed predominantly by radiative decay and significant fluorescence is detected. The overall result is a dramatic increase in fluorescence with the application of the activating optical stimulation. The main limitation of this approach, however, is that unitary quenching efficiencies in the initial state are hard, if at all possible, to achieve and only modest contrast levels are accessible. Alternative strategies to switch fluorescence from completely off to on, rather than simply from low to high intensity values, are very much needed to achieve optimal contrast.

Instead of regulating the fate of  $S_1$  with external control, fluorescence can be activated by allowing the population of this state only after the application of a chemical or optical stimulation.<sup>7</sup> Specifically, the absorption of exciting photons at  $\lambda_{\text{EX}}$  must be designed to occur exclusively after the chemical or photochemical transformation responsible for activation. Under these conditions, only the product can be excited to produce emission and fluorescence activates with infinite contrast. The implementation of such a promising mechanism requires the identification of structural designs to control the ability of a fluorescent chromophore to absorb. In this context, halochromic<sup>19</sup> and photochromic<sup>20–24</sup> compounds are particularly valuable. They alter drastically and reversibly their ability absorb visible radiation upon acidification and illumination respectively. Indeed, the integration of these functional components and complementary emissive chromophores within the same covalent backbone has been the strategy of choice in our laboratories to construct molecules capable of activating their fluorescence in response to pH and light.<sup>25,26</sup> This article overviews the structural designs and operating principles of these switchable compounds together with their application in a diversity of bioimaging experiments.

## Switchable oxazines

Nitrospiropyrans switch reversibly from a colorless state to a colored form upon ultraviolet illumination in organic solvents.<sup>27–30</sup> These photochromic transformations involve two consecutive chemical steps. First, the [C–O] bond at the spirocenter of the colorless isomer cleaves upon excitation on a picosecond timescale. Then, the adjacent [C=C] bond switches from a *cis* to a *trans* configuration to generate the colored isomer within a few microseconds. This species reverts thermally back to the original and colorless isomer after changing the configuration of the [C=C] bond from *trans* to *cis* first and then reforming the [C–O] bond. The relatively slow kinetics of the *trans* → *cis* re-isomerization, however, delays significantly the thermal decoloration process. As a result, a full switching cycle generally requires several minutes to occur. Additionally, the photoinduced step evolves predominantly along the potential-energy surface of a triplet state and, if performed in air, encourages the production of significant amounts of singlet oxygen with the concomitant degradation of the system.<sup>28</sup> In fact, nitrospiropyrans tolerate only a limited number of switching cycles.

In order to enhance the fatigue resistance and switching speeds of nitrospiropyrans, our laboratories envisaged the possibility of eliminating the need to switch the configuration of a [C=C] bond to interconvert colorless and colored species and basing these photochromic transformations exclusively on the cleavage and formation of [C–O] bond. Our studies ultimately identified a general structural design (**a** in Fig. 1) based on the fusion of 2*H*,4*H*-benzo[1,3]oxazine and 2*H*,3*H*-indole heterocycles along a [C–N] bond.<sup>31,32</sup> Illumination of these molecules at a  $\lambda_{Ac}$  in the spectral region where the 4-nitrophenoxy chromophore absorbs cleaves the [C–O] bond at the junction of the two heterocycles to generate a zwitterionic isomer (**b** in Fig. 1) on a picosecond timescale. This species reverts spontaneously back to the original isomer on timescales ranging from tens of nanoseconds to a few milliseconds, depending on the nature of the surrounding medium and substituents ( $R^1$ – $R^4$  in Fig. 1).<sup>31–40</sup> Furthermore, the photoinduced opening and thermal closing of the oxazine ring can be reiterated for hundreds of cycles without any sign of degradation, even when the system is operated in air.

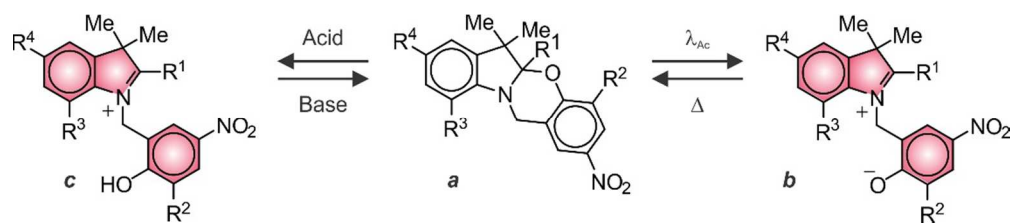


**Fig. 1.** Photochromic ( $a \rightarrow b$ ) and halochromic ( $a \rightarrow c$ ) transformations of oxazine heterocycles.

The oxazine ring of our photochromic compounds opens also upon acidification to generate the protonated form (**c** in Fig. 1) of the zwitterionic isomer.<sup>33,34</sup> Neutralization with base converts the 4-nitrophenol appendage into the 4-nitrophenolate anion of the zwitterionic species, which reverts spontaneously to the original oxazine. Thus, these particular molecules can be switched reversibly between two distinct states under the influence of either light or pH. In turn, the opening and closing of the oxazine ring can be exploited to control reversibly the photophysical properties of any given chromophoric group ( $R^1$  in Fig. 1) connected to the chiral center of the ring-closed species. Indeed, this  $sp^3$  carbon atom isolates  $R^1$  electronically from the indole heterocycle in the ground state. Opening of the oxazine ring changes the hybridization of this atom to  $sp^2$  and, only then, brings  $R^1$  in conjugation with the adjacent heterocycle. Such a structural transformation shifts bathochromically the  $S_0 \rightarrow S_1$  absorption of  $R^1$ , offering the opportunity to excite  $R^1$  selectively in the ring-open species with an appropriate  $\lambda_{EX}$  and activate fluorescence.<sup>41–49</sup>

The position of the nitro group on the phenoxy fragment of the ring-closed species controls the outcome of the photochemical transformation. Its relocation from *para* to *meta*, relative to the oxygen atom, turns the photoinduced step from reversible to irreversible. Indeed, illumination at a  $\lambda_{Ac}$  in the spectral region where the 3-nitrophenoxy absorbs cleaves the oxazine heterocycle to release a nitrosobenzaldehyde irreversibly.<sup>50</sup> In analogy to its reversible counterpart, this photochemical reaction can be exploited to control the photophysical properties of any chromophoric group ( $R^1$  in Fig. 2) attached to the chiral center of the ring-closed species. Once again, the hybridization of this carbon atom changes from  $sp^3$  to  $sp^2$  with the photoinduced transformation to bring  $R^1$  in conjugation with the adjacent heterocycle. As a result, the  $S_0 \rightarrow S_1$  absorption of  $R^1$  shifts bathochromically, allowing its

selective excitation within the photochemical product and the irreversible activation of its fluorescence.<sup>50–54</sup>

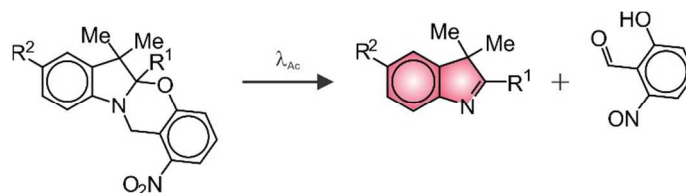


**Fig. 2.** Photoinduced and irreversible cleavage of oxazine heterocycles.

### Reversible fluorescence photoactivation

Fluorescent chromophores with a formyl substituent can be connected to our switchable oxazines in a single synthetic step.<sup>41,42,47</sup> Compound **1a** (Fig. 3) is a representative example of these fluorophore–photochrome dyads.<sup>41,42</sup> Its coumarin fluorophore and oxazine auxochrome are isolated electronically in the ground state. As a result, the absorption spectrum of **1a** in acetonitrile shows the characteristic coumarin absorption at 412 nm (**a** in Fig. 3). Illumination at a  $\lambda_{Ac}$  of 355 nm, where the 4-nitrophenoxy fragment absorbs, opens the oxazine ring to produce **1b**. This structural transformation brings the coumarin chromophore in electronic conjugation with the indolium auxochrome to shift its  $S_0 \rightarrow S_1$  absorption to 570 nm (**b** in Fig. 3). Irradiation at a  $\lambda_{Ex}$  of 532 nm excites selectively the photochemical product with concomitant fluorescence 650 nm (**c** in Fig. 3). Indeed, the bathochromic shift in absorption imposed on the coumarin component with the photoinduced transformation translates into fluorescence activation with infinite contrast.

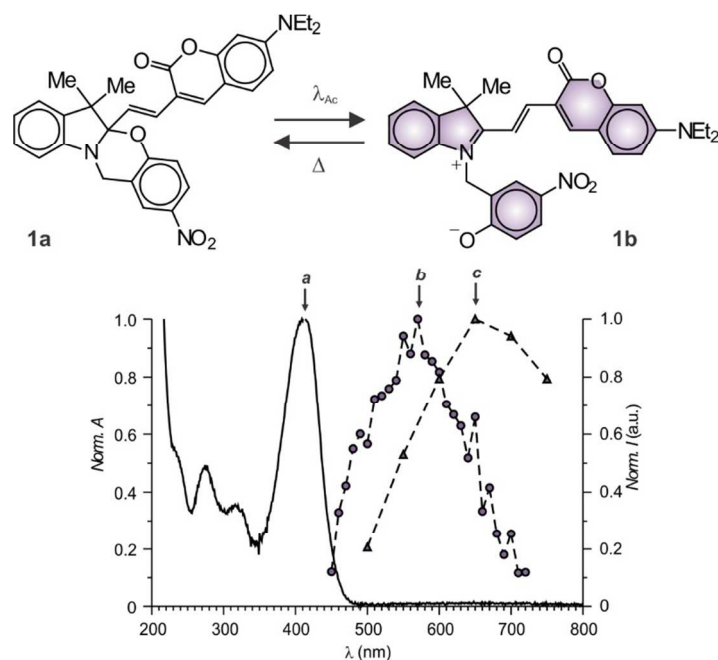


**Fig. 3.** Absorption (**a** and **b**) and emission (**c**,  $\lambda_{Ex} = 532$  nm) spectra of an acetonitrile solution of **1a** recorded before (**a**) and after (**b** and **c**) irradiation ( $\lambda_{Ac} = 355$  nm).

The photogenerated and zwitterionic species reverts spontaneously to the ring-closed isomer on a microsecond timescale in acetonitrile.<sup>41,42</sup> Consistently, the absorption band of the coumarin fluorophore shifts back to the original position, preventing the absorption of photons at  $\lambda_{Ex}$  and turning fluorescence off. Furthermore, this particular photochromic system retains the excellent fatigue resistance designed into the oxazine component and can be switched for hundreds of cycles without any sign of degradation. As a result, the reversible and continuous interconversion of **1a** and **1b** translates into fluorescence intermittency. Emission turns on with the photoinduced formation of **1b** and then off with the thermal regeneration of **1a**. Indeed, fluorescence blinking at the single-molecule level is evident when this photoactivatable fluorophore is entrapped into a rigid polymer matrix to prevent diffusion.<sup>42</sup> In turn, the blinking of individual emitters allows their differentiation in time, even when they are closely spaced, and the sequential localization of their positions within the sample. On the basis of this protocol, images with spatial resolution below the diffraction limit can ultimately be reconstructed.

The introduction of an active ester in position 5 of the indole heterocycle of **1a** permits the covalent connection of this photoactivatable fluorophore to antibodies, under standard amide-coupling conditions.<sup>48</sup> For example, a secondary antibody, capable of staining the tubulin structure of fixed cells with conventional immunolabeling protocols, can be paired with the photoresponsive compound in the shape of **2a** (Fig. 4). The fluorescence intermittency of the resulting bioconjugate then allows the visualization of the tubulin filaments with nanoscaled resolution. Indeed, comparison of a conventional diffraction-limited image (**a** in Fig. 4) of the sample to a subdiffraction counterpart (**b** in Fig. 4), reconstructed from 83,000 frames collected sequentially while switching the emissive probes on and off, reveals the significant enhancement in spatial resolution accessible as a result of fluorescence activation. Only in the reconstructed image can the nanostructured filaments be clearly distinguished.

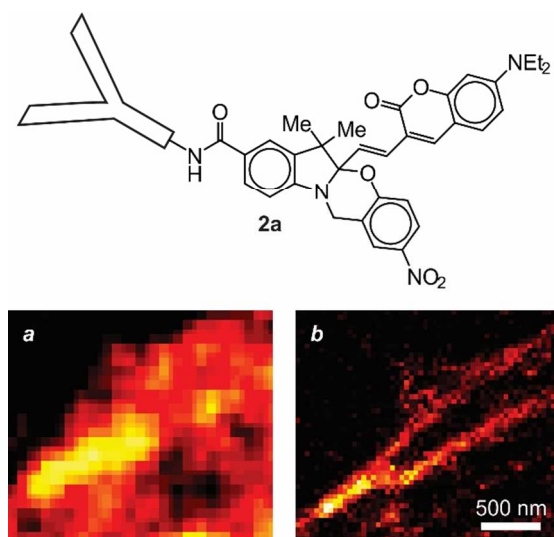


**Fig. 4.** Diffraction-limited (**a**) and subdiffraction (**b**) fluorescence images ( $\lambda_{Ac} = 405$  nm;  $\lambda_{Ex} = 532$  nm) of fixed cells (VERO) immunolabeled with **2a**.

### pH-induced fluorescence activation

The operating principles to control the spectral position of the  $S_0 \rightarrow S_1$  absorption of a fluorescent chromophore with light can be replicated under the influence of pH with essentially the same structural design.<sup>42–49</sup> For example, addition of one equivalent of trifluoroacetic acid to an acetonitrile solution of **1a** also opens the oxazine ring to generate the protonated form of the zwitterionic isomer, in the shape of **1c** (Fig. 5).<sup>44</sup> This structural transformation also brings the coumarin fluorophore in electronic

conjugation with the indolium auxochrome to produce the very same extended chromophoric fragment of the photogenerated species (*cf.* **1b** and **1c**). As a result, the absorption band of the coumarin fluorophore shifts from 412 to 593 nm (**a** and **b** in Fig. 5) upon acidification. In analogy to the photoinduced transformation, this pronounced bathochromic shift offers the opportunity to excite selectively the protonated form at a  $\lambda_{\text{EX}}$  of 590 nm to produce fluorescence at 685 nm (**c** in Fig. 5).

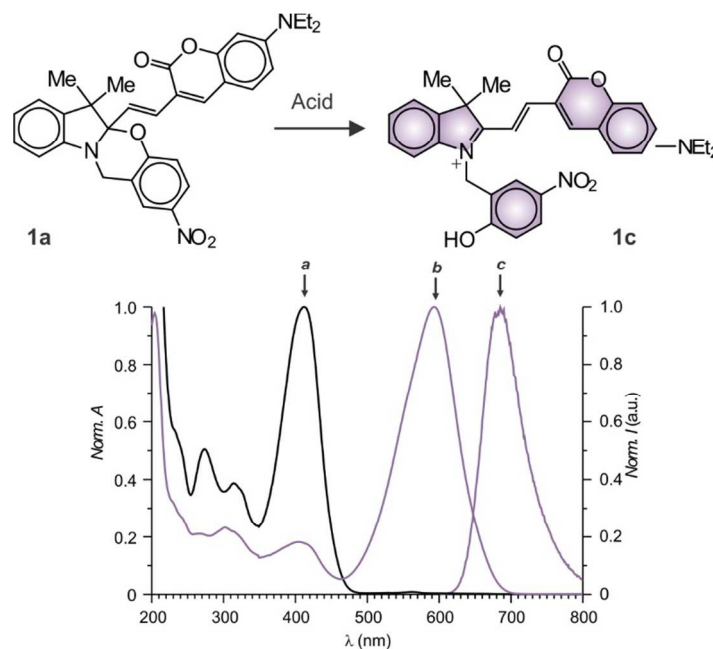


**Fig. 5.** Absorption and emission spectra of an acetonitrile solution of **1a** recorded before (**a**) and after (**b** and **c**,  $\lambda_{\text{EX}} = 590$  nm) addition of trifluoroacetic acid (1 eq.).

The ability to activate fluorescence with pH is particularly valuable to generate emissive probes exclusively in the intracellular environment of target cells.<sup>55–58</sup> Indeed, receptor-mediated endocytosis can be exploited to direct pH-activatable fluorophores into acidic intracellular compartments with the aid of appropriate targeting ligands.<sup>59–62</sup> For example, the folate receptor can transport derivatives of folic acid from the neutral extracellular matrix into acidic endosomes.<sup>63–66</sup> This receptor is overexpressed on the surface of most cancer cells and, therefore, its endocytic pathway can be relied upon to promote the selective internalization of fluorophores into malignant cells and allow their discrimination over normal counterparts. The mechanism to switch fluorescence engineered into **1a** is especially convenient in this context.

Derivatives of our coumarin–oxazine dyad and folic acid can be integrated within the same covalent construct to form **3a** (Fig. 6) in three synthetic steps.<sup>49</sup> The resulting macromolecule incorporates hydrophilic oligo(ethylene glycol) and hydrophobic decyl side chains along a common poly(methacrylate) backbone. The oligo(ethylene glycol) tails impose aqueous solubility on the overall assembly. Additionally, some of them bear folate ligands at their ends to encourage the association of the macromolecule to the folate receptor. The decyl chains are terminated with the pH-activatable dyads that are required to produce fluorescence after cellular internalization. Furthermore, they provide a hydrophobic environment to the chromophoric components to insulate them effectively from each other and preserve their photophysical properties. In analogy to the behavior of **1a**, acidification of aqueous solutions of this macromolecular construct opens the oxazine rings of the signaling units to shift bathochromically the coumarin absorption and allow the selective excitation of the protonated species. As a result, fluorescence turns on with infinite contrast as the pH of the solution lowers below 5. Interestingly, the brightness of this system in acidic environments is *ca.* 170 times greater than that of an individual coumarin–oxazine dyad. The remarkable enhancement is a consequence of significant increases in both molar absorption coefficient and fluorescence quantum yield, relative to an isolated fluorophore. The presence of multiple chromophoric units in the same construct and the relatively constrained environment within the polymer are responsible for the increase of these two photophysical parameters respectively. Indeed, the restricted conformational freedom imposed by the macromolecular construct on the extended chromophoric platform of the protonated fluorophore discourages nonradiative pathways that would, otherwise, dominate the decay of the excited state and depress significantly the quantum efficiency of the emission process.

Incubation of folate-receptor negative and positive cells with **3a** results in significant intracellular fluorescence only for the latter (**a** and **b** in Fig. 6).<sup>49</sup> Indeed, the macromolecular construct associates with the folate receptors overexpressed on the cell surface first and then internalizes into acidic organelles, where the signaling units switch their fluorescence on and allow the visualization of the cells against an essentially dark background. Additionally, the emission intensity detected in the intracellular environment increases with the incubation time, as the concentration of internalized

polymer raises, while it remains negligible for the receptor-negative cells. In further support of the role of the folate receptor in promoting the internalization of the activatable units, inhibition experiments suppress completely the intracellular fluorescence. Specifically, folate-receptor positive cells pre-treated with folic acid and then incubated with **3a** do not show any intracellular fluorescence. In fact, folic acid associates with the folate receptors and prevents binding and internalization of **3a**.

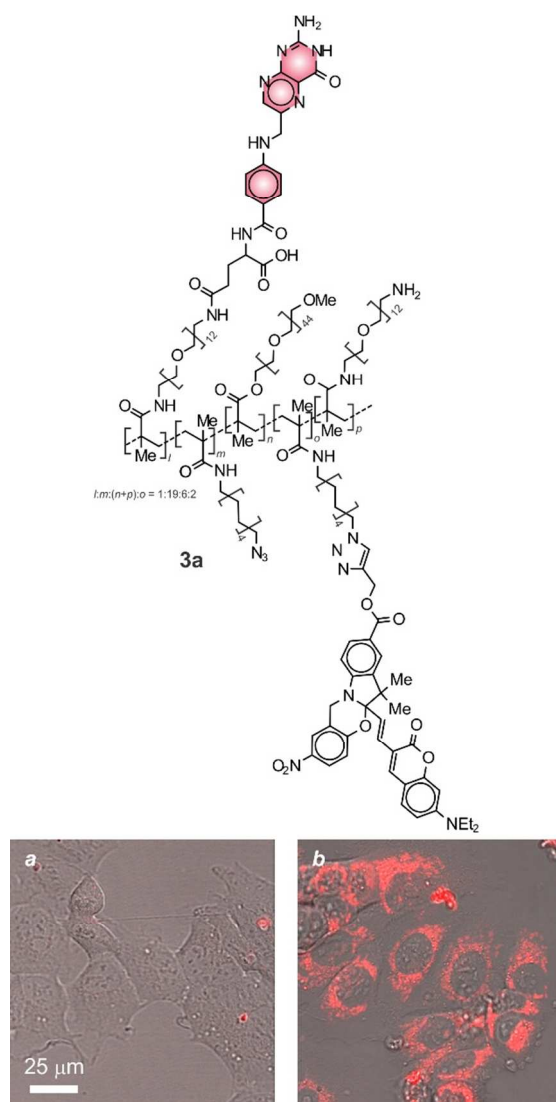


**Fig. 6.** Overlaps of brightfield and fluorescence ( $\lambda_{\text{EX}} = 561 \text{ nm}$ ) images of folate-receptor negative (**a**, HEK-293) and folate-receptor positive (**b**, MCF-7) cells incubated with **3a** for 2 hours.

### Irreversible fluorescence photoactivation

The nitro substituent on the phenoxy fragment of our switchable oxazines can be relocated from position 4 to position 3, relative to the oxygen atom, to produce an *ortho*-nitrobenzyl fragment. In turn, the proximity of methylene and nitro groups on *ortho*-nitrobenzyl derivatives is known to promote the cleavage of the benzylic bond, upon excitation, to form the corresponding *ortho*-nitrosobenzaldehyde.<sup>67</sup> Indeed, numerous photocaged compounds for a diversity of applications have been designed already around these particular photocleavable protecting groups and established photochemical reaction.<sup>68</sup> The excitation dynamics of the *ortho*-nitrobenzyl group are retained also when it is incorporated within our switchable oxazines to allow their irreversible photoinduced transformation.<sup>50–54</sup> Compound **4a** (Fig. 7) is a representative example of this structural design.<sup>52</sup> Illumination at a  $\lambda_{Ac}$  of 350 nm, where the *ortho*-nitrobenzyl group absorbs significantly, disconnects the oxazine heterocycle irreversibly to generate **4b**. In analogy to the behavior of **1a**, the photochemical transformation converts the  $sp^3$  chiral center of the oxazine heterocycle into a  $sp^2$  carbon atom in the product. As a result, only then can the borondipyrromethene (BODIPY) chromophore delocalize its electrons over the adjacent acetylenic auxochrome with a concomitant bathochromic shift in absorption from 548 nm in **4a** to 600 nm in **4b** (**a** and **b** in Fig. 7) in acetonitrile. While the absorption of the coumarin appendage of **1a** shifts into a spectral window compatible with bioimaging applications only after the formation of **1b**, the band of the BODIPY chromophore of **4a** is already positioned in the visible region and can be exploited to generate fluorescence with excitation wavelengths that ensure negligible autofluorescence in biological specimens. It follows that the photoinduced transformation of **4a** into **4b** provides the opportunity to switch the color of fluorescence, rather than turning its intensity from off to on. In fact, excitation of the reactant before and of the product after activation results in the detection of emission bands at 561 and 625 nm (**c** and **d** in Fig. 7) respectively.

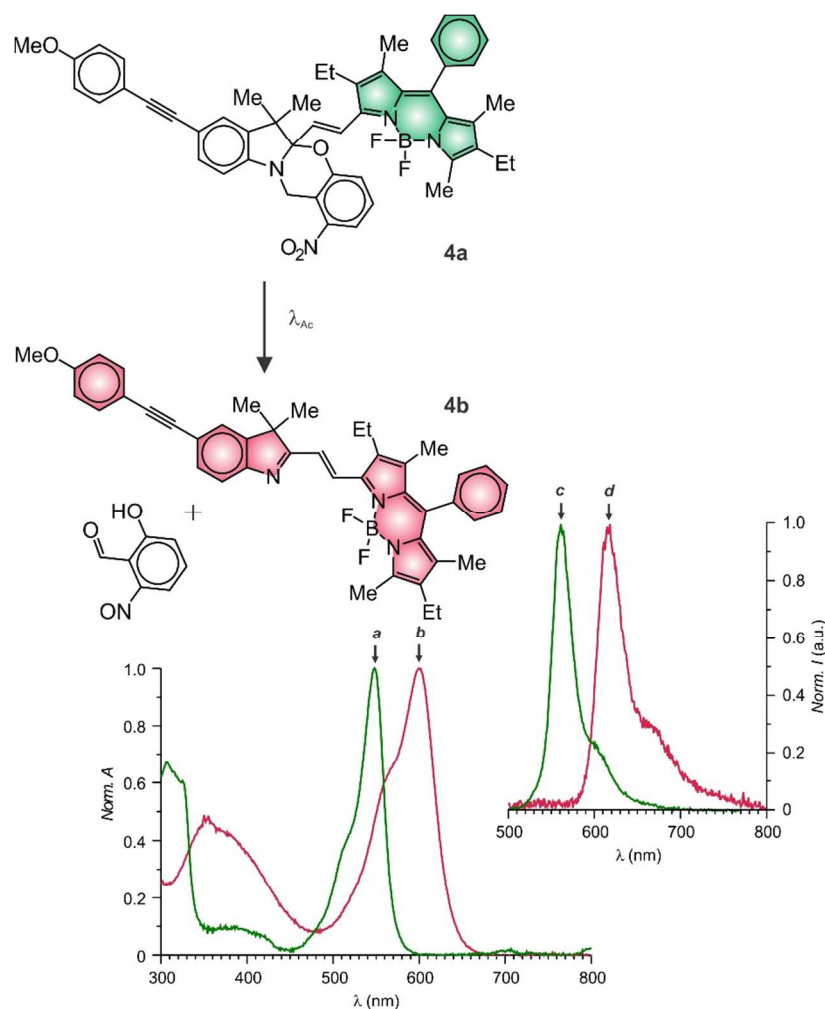


**Fig. 7.** Absorption and emission spectra of acetonitrile solutions of **4a** (**a** and **c**,  $\lambda_{Ex} = 480$  nm) and **4b** (**b** and **d**,  $\lambda_{Ac} = 350$  nm,  $\lambda_{Ex} = 540$  nm).

The absorption of the *ortho*-nitrobenzyl fragment of **4a** tails into the visible region of the electromagnetic spectrum, enabling activation with a laser line of 405 nm.<sup>52</sup> The visible wavelength and mild illumination sufficient to induce the photochemical conversion of this compound offer the opportunity to switch fluorescence *in vivo*. Specifically, **4a** can be injected into *Drosophila melanogaster* embryos at early stages of their development. The relatively hydrophobic BODIPY-oxazine dyads localize into the membranes of the cellular blastoderm,<sup>69</sup> allowing their visualization. Indeed, an image (**a** in Fig. 8) acquired exciting the BODIPY fluorophore of **4a** at a  $\lambda_{Ex}$  of 514 nm and collecting its fluorescence between 525 and 600 nm clearly shows the membranes of the many cells in the blastoderm.<sup>52</sup> Irradiation of a portion of the blastoderm at a  $\lambda_{Ac}$  of 405 nm switches **4a** into **4b**.

Consistently, an image (**b** in Fig. 8), recorded under the same excitation and detection conditions, reveals a significant decrease in the fluorescence of **4a** exclusively in the activated area. The photochemical product can be excited selectively at a  $\lambda_{\text{Ex}}$  of 633 nm to collect its emission in a separate detection channel between 640 and 750 nm. Comparison of images (**c** and **d** in Fig. 8), acquired under these conditions before and after activation, clearly shows the appearance of the fluorescence of the product. The developing fluorescence is localized, once again, in the membranes of the cellular blastoderm. However, the hydrophobic fluorescent probes can diffuse through the hydrophobic network of contacting membranes in the blastoderm. As a result, images collected sequentially, after activation, permit the tracking of the translocating probes in real time for prolonged periods of time, demonstrating that the operating principles for fluorescence switching designed into our BODIPY–oxazine dyad allow the monitoring of dynamic events in living organisms.

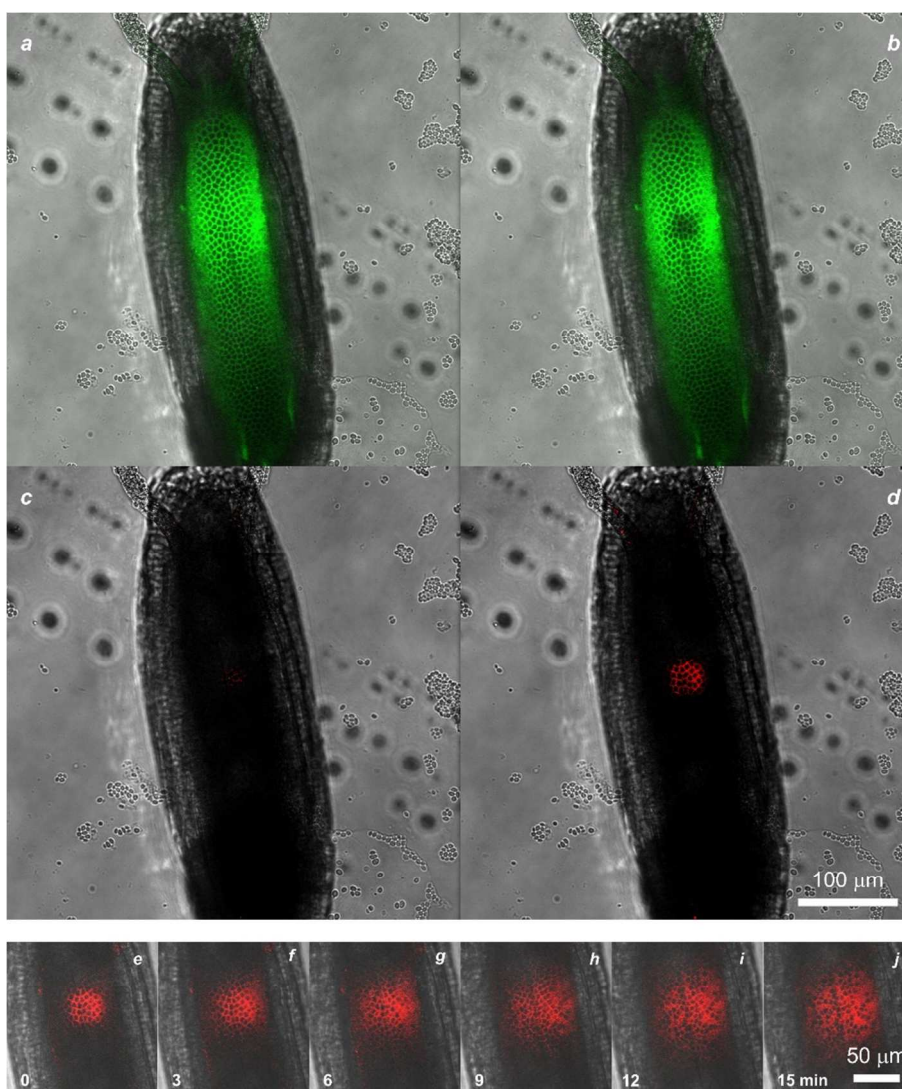


**Fig. 8.** Overlaps of brightfield and fluorescence images of *Drosophila melanogaster* embryos injected with **4a** recorded before (**a**,  $\lambda_{\text{Ex}} = 514 \text{ nm}$ ,  $\lambda_{\text{Em}} = 525\text{--}600 \text{ nm}$ ; **c**,  $\lambda_{\text{Ex}} = 633 \text{ nm}$ ,  $\lambda_{\text{Em}} = 640\text{--}750 \text{ nm}$ ) and after (**b**,  $\lambda_{\text{Ex}} = 514 \text{ nm}$ ,  $\lambda_{\text{Em}} = 525\text{--}600 \text{ nm}$ ; **d**,  $\lambda_{\text{Ex}} = 633 \text{ nm}$ ,  $\lambda_{\text{Em}} = 640\text{--}750 \text{ nm}$ ) illumination ( $\lambda_{\text{Ac}} = 405 \text{ nm}$ ) of part of the cellular blastoderm and over the course of the subsequent 15 min (**e–j**,  $\lambda_{\text{Ex}} = 633 \text{ nm}$ ,  $\lambda_{\text{Em}} = 640\text{--}750 \text{ nm}$ ).

The mechanism responsible for the irreversible interconversion of two species with resolved emission can be adapted to implement operating principles for three-color switching.<sup>54</sup> Specifically, the BODIPY fluorophore can be paired covalently to two switchable oxazines in the shape of **5a** (Fig. 9). Illumination at a  $\lambda_{\text{Ac}}$  in the spectral region where the two *ortho*-nitrobenzyl fragments absorb results in the stepwise formation **5b** and **5c** (Fig. 9). The first photochemical step brings the BODIPY

chromophore in electronic conjugation with one indole auxochrome and shifts its absorption band from 574 to 619 nm (**a** and **b** in Fig. 9) in acetonitrile. The second reaction extends electronic delocalization even further and shifts the absorption to 663 nm (**c** in Fig. 9). In fact, the two consecutive photoinduced structural changes shift bathochromically also the emission band, which moves from 587 to 628 nm first and then further to 673 nm (**d–f** in Fig. 9).

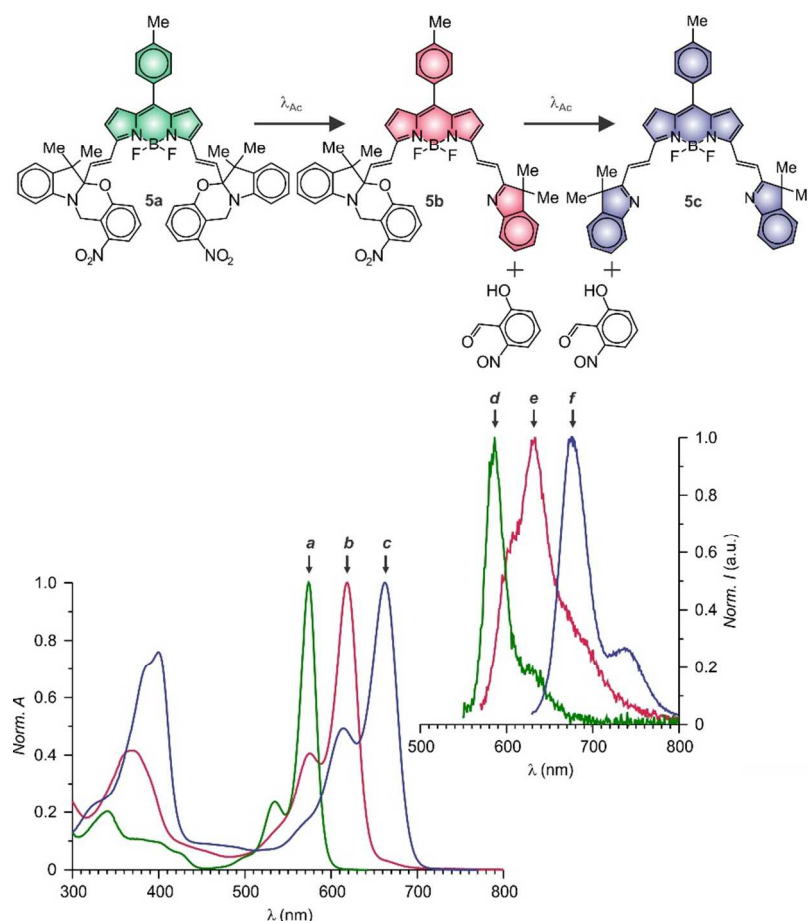


**Fig. 9.** Absorption and emission spectra of acetonitrile solutions of **5a** (**a** and **d**,  $\lambda_{Ex} = 540$  nm), **5b** (**b** and **e**,  $\lambda_{Ac} = 350$  nm,  $\lambda_{Ex} = 560$  nm) and **5c** (**c** and **f**,  $\lambda_{Ac} = 350$  nm,  $\lambda_{Ex} = 620$  nm).

The emission bands of **5a**, **5b** and **5c** are sufficiently resolved across the visible region to enable the collection of their fluorescence in three separate detection channels of a single laser-scanning confocal microscope.<sup>54</sup> Furthermore, the same absorption profile of the two identical *ortho*-nitrobenzyl groups offers the opportunity to induce the two photochemical steps at the same  $\lambda_{Ac}$  with a single laser source. In fact, the relative amounts of **5a**, **5b** and **5c**, and, hence, their relative emission intensities, in a

specific area of any given sample of interest can be regulated precisely simply by adjusting the dose of activating photons. For example, microscaled polystyrene beads can be doped with **5a**, deposited on a glass slide and illuminated individually at  $\lambda_{Ac}$  with identical power but for different times. Under these conditions, the initially identical beads can be marked photochemically with distinct fluorescent signals to allow their differentiation.

The mild visible illumination sufficient to induce the two consecutive photochemical reactions permits the implementation of this photochemical strategy for signal encoding *in vivo*.<sup>54</sup> Furthermore, the relatively long excitation and emission wavelengths of the three species enable the acquisition of their fluorescence in biological samples with negligible autofluorescence. For example, *Caenorhabditis elegans* can be labeled with polystyrene beads, doped with **5a**, and then treated with muscimol, a GABA-A receptor agonist.<sup>70</sup> Under these conditions, the worms remain paralyzed for a sufficiently long time<sup>71</sup> to enable the illumination of distinct positions of their body at  $\lambda_{Ac}$  with an increasing dose of activating photons. The resulting specimens can then be imaged in brightfield mode and three fluorescence channels in parallel to localize the emissive objects. Overlaps of the resulting images for the tail and head sections (**a** and **b** in Fig. 10) of one worm, together with the corresponding magnifications (**c–g** in Fig. 10), clearly reveal fluorescence with different colors in the illuminated areas. Furthermore, the emission intensity can be quantified in each one of the three detection channels for each one of the illuminated areas and then plotted ratiometrically to eliminate inconsistencies in the dopant loading and physical dimensions across the polymer beads. The resulting bars (**h** in Fig. 10) demonstrate that each illuminated area has a unique code of three fluorescence signals. Furthermore, such photochemically imprinted barcodes remain stable for prolonged periods of time and enable the tracking of dynamic events in the labeled animal. Indeed, the paralyzed animal resumes normal activity within a few hours, once the effect of muscimol fades away.<sup>71</sup> At this point, pharyngeal pumping forces the fluorescent beads to move along the intestinal tract of the animal and their translocation can be tracked in real time with the sequential acquisition fluorescence images in the three channels to read the imprinted barcodes.

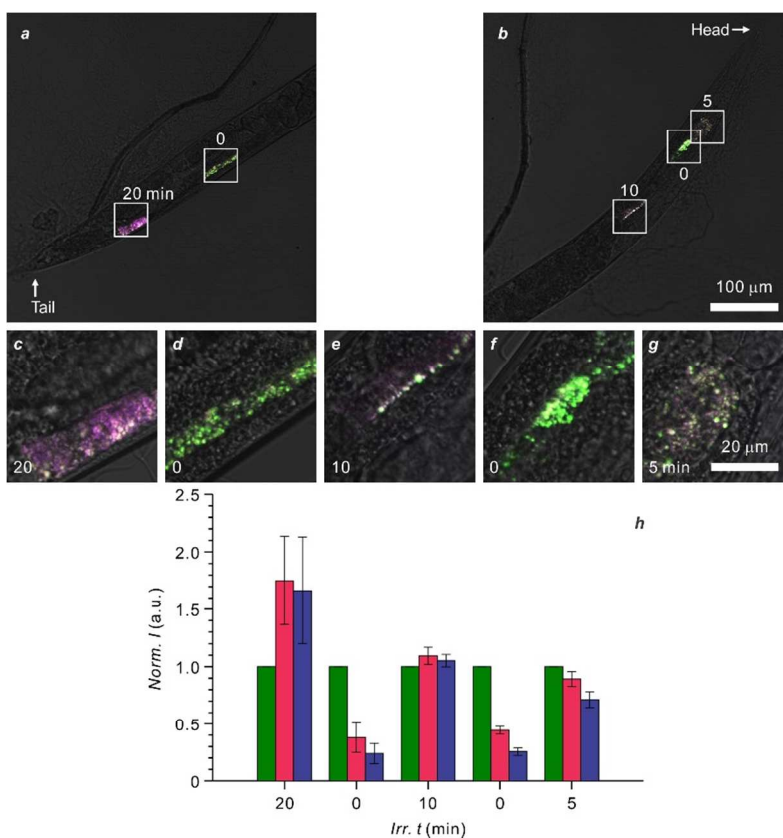


**Fig. 10.** Overlaps of brightfield and fluorescence images (Green:  $\lambda_{\text{Ex}} = 561$  nm,  $\lambda_{\text{Em}} = 575\text{--}600$  nm; Red:  $\lambda_{\text{Ex}} = 633$  nm,  $\lambda_{\text{Em}} = 645\text{--}660$  nm; Blue:  $\lambda_{\text{Ex}} = 633$  nm,  $\lambda_{\text{Em}} = 750\text{--}800$  nm;) of *Caenorhabditis elegans* labeled with PS beads, doped with **5a**, recorded after irradiation ( $\lambda_{\text{Ac}} = 405$  nm) of distinct regions for different times, magnifications of non-irradiated (**d** and **f**) and irradiated (**c**, **e** and **g**) areas and relative emission intensities (**h**).

## Conclusions

Benzo[1,3]oxazine heterocycles with a nitro substituent in the *para* position, relative to the oxygen atom, open reversibly in response to either light or pH. Relocation of the nitro group to the *meta* position cleaves them irreversibly under illumination. In all instances, the carbon atom bridging the oxygen and nitrogen atoms of the [1,3]oxazine heterocycle switches hybridization from  $sp^3$  to  $sp^2$ . This structural transformation can be exploited to extend the electronic delocalization of any chromophoric groups connected to this carbon and shift bathochromically its  $S_0 \rightarrow S_1$  absorption. In turn, such a spectral shift enables the selective excitation of the resulting species with concomitant fluorescence

activation. When this process is performed reversibly under the influence of light, fluorescence switches back off with the reformation of the oxazine ring. As a result, intermittency can be imposed on the emission detected at the single-molecule level to allow the temporal separation of even closely-spaced fluorophores and the reconstruction of images with subdiffraction resolution. When fluorescence activation occurs in response to pH, targeting ligands can be connected to the switchable fluorophores to direct them selectively into acidic intracellular compartments. Under these conditions, the intracellular environment of malignant cells can be marked with emissive probes to allow their visualization against a nonemissive background. When fluorescence activation is performed irreversibly under the influence of light, the fluorescent species persists for prolonged periods of time. As a result, the dynamics of the photogenerated species can be monitored *in vivo* with the sequential acquisition of images after a single activation event. These promising imaging techniques are only possible because of the spatiotemporal control of emission accessible with these switchable compounds and, hence, cannot be otherwise performed with conventional fluorophores. Thus, the photochemical and photophysical properties engineered into our molecular switches are particularly valuable for the implementation of bioimaging strategies and can evolve into an entire family of activatable probes for a diversity of applications in the biomedical laboratory.

## Acknowledgments

The National Science Foundation (CHE-1505885) is acknowledged for financial support.

## References

- 1 J. R. Lakowicz, *Principles of Fluorescence Spectroscopy*, Springer, New York, 2006.
- 2 L. M. Wysocki and L. D. Lavis, *Curr. Op. Chem. Biol.*, 2011, **15**, 752–759.
- 3 D. Puliti, D. Warther, C. Orange, A. Specht and M. Goeldner, *Bioorg. Med. Chem.*, 2011, **19**, 1023–1029.
- 4 W. H. Li and G. Zheng, *Photochem. Photobiol. Sci.*, 2012, **11**, 460–471.

- 5 F. M. Raymo, *J. Phys. Chem. Lett.*, 2012, **3**, 2379–2385.
- 6 P. Klán, T. Šolomek, C. G. Bochet, A. Blanc, R. Givens, M. Rubina, V. Popik, A. Kostikov and J. Wirz, *Chem. Rev.*, 2013, **113**, 119–191.
- 7 F. M. Raymo, *Phys. Chem. Chem. Phys.*, 2013, **15**, 14840–14850.
- 8 S. Lee, J. Xie and X. Chen, *Curr. Top. Med. Chem.*, **2010**, *10*, 1135–1144.
- 9 T. W. B. Liu, J. Chen and G. Zheng, *Amino Acids*, **2011**, *41*, 1123–1134.
- 10 A. B. Chinen, C. M. Guan, J. R. Ferrer, S. N. Barnaby, T. J. Merkel and C. A. Mirkin, *Chem. Rev.*, **2015**, *115*, 10530–10574.
- 11 J. Li, F. Cheng, H. Huang, L. Li and J.-J. Zhu, *Chem. Soc. Rev.*, **2015**, *44*, 7855–7880.
- 12 R. W. Dirks, C. Molenaar and H. J. Tanke, *Histochem. Cell Biol.*, 2001, **115**, 3–11.
- 13 G. C. Ellis-Davies, *Nat. Methods*, 2007, **4**, 619–628.
- 14 Y. Xu, T. J. Melia and D. T. Toomre, *Curr. Op. Chem. Biol.*, 2011, **15**, 822–830.
- 15 F. M. Raymo, *ISRN Phys. Chem.*, 2012, 619251-1–15.
- 16 E. Betzig, *Angew. Chem. Int. Ed.*, 2015, **54**, 8034–8053.
- 17 S. W. Hell, *Angew. Chem. Int. Ed.*, 2015, **54**, 8054–8066.
- 18 W. E. Moerner, *Angew. Chem. Int. Ed.*, 2015, **54**, 8067–8093.
- 19 P. Muller, *Pure Appl. Chem.*, 1994, **66**, 1077–1184.
- 20 M. Irie (Ed.), *Chem. Rev.*, 2000, **100**, 1683–1890.
- 21 D. Bassani, J. Hofkens and J. L. Pozzo (Eds.), *Photochem. Photobiol. Sci.*, 2010, **9**, 117–264.

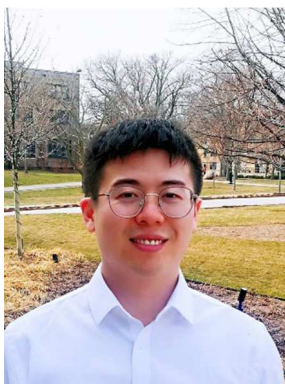
- 22 G. Favaro and M. Irie (Eds.), *J. Photochem. Photobiol. C*, 2011, **12**, 71–236.
- 23 F. M. Raymo and D. Gust, *Isr. J. Chem.*, 2013, **53**, 229–311.
- 24 M. Irie, M. Yokoyama and Y. Seki (Eds.), *New Frontiers in Photochromism*, Springer, New York, 2013.
- 25 E. Deniz, M. Tomasulo, J. Cusido, S. Sortino and F. M. Raymo, *Langmuir*, 2011, **27**, 11773–11783.
- 26 F. M. Raymo, *Isr. J. Chem.*, 2013, **53**, 247–255.
- 27 G. Berkovic, V. Krongauz and V. Weiss, *Chem. Rev.*, 2000, **100**, 1741–1754.
- 28 H. Görner, *Phys. Chem. Chem. Phys.*, 2001, **3**, 416–423.
- 29 V. I. Minkin, *Chem. Rev.*, 2004, **104**, 2751–2776.
- 30 R. Klajn, *Chem. Soc. Rev.*, 2014, **43**, 148–184.
- 31 M. Tomasulo, S. Sortino and F. M. Raymo, *Org. Lett.*, 2005, **7**, 1109–1112.
- 32 M. Tomasulo, S. Sortino, A. J. P. White and F. M. Raymo, *J. Org. Chem.*, 2005, **70**, 8180–8189.
- 33 M. Tomasulo, S. Sortino and F. M. Raymo, *Adv. Mater.*, 2008, **20**, 832–835.
- 34 M. Tomasulo, S. Sortino and F. M. Raymo, *J. Org. Chem.*, 2008, **73**, 118–126.
- 35 E. Deniz, M. Tomasulo, S. Sortino and F. M. Raymo, *J. Phys. Chem. C*, 2009, **113**, 8491–8497.
- 36 M. Tomasulo, E. Deniz, S. Sortino and F. M. Raymo, *Photochem. Photobiol. Sci.*, 2010, **9**, 136–140.
- 37 E. Deniz, S. Sortino and F. M. Raymo, *J. Phys. Chem. Lett.*, 2010, **1**, 1690–1693.

- 38 E. Deniz, S. Ray, M. Tomasulo, S. Impellizzeri, S. Sortino and F. M. Raymo, *J. Phys. Chem. A*, 2010, **114**, 11567–11575.
- 39 E. Deniz, S. Impellizzeri, S. Sortino and F. M. Raymo, *Can. J. Chem.*, 2011, **89**, 110–116.
- 40 S. Swaminathan, J. Garcia-Amorós, E. R. Thapaliya, S. Nonell, B. Captain and F. M. Raymo, *ChemPhysChem*, 2016, **17**, 1852–1859.
- 41 E. Deniz, S. Sortino and F. M. Raymo, *J. Phys. Chem. Lett.*, 2010, **1**, 3506–3509.
- 42 E. Deniz, M. Tomasulo, J. Cusido, I. Yildiz, M. Petriella, M. L. Bossi, S. Sortino and F. M. Raymo, *J. Phys. Chem. C*, 2012, **116**, 6058–6068.
- 43 J. Cusido, M. Battal, E. Deniz, I. Yildiz, S. Sortino and F. M. Raymo, *Chem. Eur. J.*, 2012, **18**, 10399–10407.
- 44 S. Swaminathan, M. Petriella, E. Deniz, J. Cusido, J. D. Baker, M. L. Bossi and F. M. Raymo, *J. Phys. Chem. A*, 2012, **116**, 9928–9933.
- 45 E. Deniz, N. Kandoth, A. Fraix, V. Cardile, A. C. E. Graziano, D. Lo Furno, R. Gref and F. M. Raymo, S. Sortino, *Chem. Eur. J.*, 2012, **18**, 15782–15787.
- 46 M. Petriella, E. Deniz, S. Swaminathan, M. J. Roberti, F. M. Raymo and M. L. Bossi, *Photochem. Photobiol.*, 2013, **89**, 1391–1398.
- 47 J. Garcia-Amorós, S. Swaminathan, S. Sortino and F. M. Raymo, *Chem. Eur. J.*, 2014, **20**, 10276–10284.
- 48 J. Cusido, S. Shaban Ragab, E. R. Thapaliya, S. Swaminathan, J. Garcia-Amorós, M. J. Roberti, B. Araoz, M. M. A. Mazza, S. Yamazaki, A. M. Scott, F. M. Raymo and M. L. Bossi, *J. Phys. Chem. C*, 2016, **120**, 12860–12870.

- 49 S. Tang, Y. Zhang, E. R. Thapaliya, A. S. Brown, J. N. Wilson and F. M. Raymo, *ACS Sens.*, 2017, **2**, 92–101.
- 50 Y. Zhang, S. Swaminathan, S. Tang, J. Garcia-Amorós, M. Boulina, B. Captain, J. D. Baker and F. M. Raymo, *J. Am. Chem. Soc.*, 2015, **137**, 4709–4719.
- 51 J. Garcia-Amorós, S. Swaminathan, Y. Zhang, S. Nonell and F. M. Raymo, *Phys. Chem. Chem. Phys.*, 2015, **17**, 11140–11143.
- 52 Y. Zhang, S. Tang, L. Sansalone, J. D. Baker and F. M. Raymo, *Chem. Eur. J.*, 2016, **22**, 15027–15034.
- 53 X. Liu, Y. Zhang, J. D. Baker and F. M. Raymo, *J. Mater. Chem. C*, 2017, **5**, 12714–12719.
- 54 S. Tang, Y. Zhang, P. Dhakal, L. Ravelo, C. L. Anderson, K. M. Collins and F. M. Raymo, *J. Am. Chem. Soc.*, 2018, **140**, 4485–4488.
- 55 J. Han and K. Burgess, *Chem. Rev.*, 2010, **110**, 2709–2728.
- 56 R. Wang, C. Yu, F. Yu and L. Chen, *Trac-Trend Anal. Chem.*, 2010, **29**, 1004–1013.
- 57 X. H. Li, X. H. Gao, W. Shi and H. M. Ma, *Chem. Rev.*, 2014, **114**, 590–659.
- 58 J.-T. Hou, W. X. Ren, K. Li, J. Seo, A. Sharma, X.-Q. Yu and J. S. Kim, *Chem. Soc. Rev.*, 2017, **46**, 2076–2090.
- 59 G. J. Doherty and H. T. McMahon, *Annu. Rev. Biochem.*, 2009, **78**, 857–902.
- 60 H. T. McMahon and E. Boucrot, *Nat. Rev. Mol. Cell Biol.*, 2011, **12**, 517–533.
- 61 I. Canton and G. Battaglia, *Chem. Soc. Rev.*, 2012, **41**, 2718–2739.
- 62 O. L. Mooren, B. J. Galletta and J. A. Cooper, *Ann. Rev. Biochem.*, 2012, **81**, 661–686.

- 63 Y. J. Lu and P. S. Low, *Adv. Drug Deliv. Rev.*, 2012, **64**, 342–352.
- 64 I. R. Vlahov and C. P. Leamon, *Bioconjugate Chem.*, 2012, **23**, 1357–1369.
- 65 I. B. Vergote, C. Marth and R. L. Coleman, *Cancer Metastasis Rev.*, 2015, **34**, 41–52.
- 66 R. J. Lutz, *Transl. Cancer Res.*, 2015, **4**, 118–126.
- 67 A. P. Pelliccioli and J. Wirz, *Photochem. Photobiol. Sci.*, 2002, **1**, 441–458.
- 68 M. Goeldner and R. Givens (Eds.), *Dynamic Studies in Biology: Phototriggers, Photoswitches and Caged Biomolecules*, Wiley–VCH, Weinheim, 2005.
- 69 Y. Zhang, E. R. Thapaliya, S. Tang, J. D. Baker and F. M. Raymo, *RSC Adv.*, 2016, **6**, 72756–72760.
- 70 C. Fang-Yen, L. Avery and A. D. Samuel, *Proc. Natl. Acad. Sci. U.S.A.*, 2009, **106**, 20093–20096.
- 71 K. M. Collins and M. R. Koelle, *J Neurosci.*, 2013, **33**, 761–775.

### Biographical sketches



Yang Zhang received a B.Sc. in Chemistry from Qilu University of Technology (China) in 2012 and a Ph.D. in Chemistry, under the guidance of Professor Raymo, from the University of Miami in 2017. His graduate research involved the design of photoswitchable fluorophores, based on BODIPY derivatives, and the development of supramolecular delivery strategies for bioimaging applications. He was appointed postdoctoral fellow at Northwestern University in 2017. His present research interests focus on the development of novel synthetic fluorescent probes for spectroscopic single-molecule localization microscopy and multi-dimensional super-resolution imaging. He has authored 24 publications in the general areas of fluorescence imaging, materials science, molecular switches and photochemistry.



Sicheng Tang received a B.Sc. in Materials Chemistry from Jilin University (China) in 2013 and a Ph.D. in Chemistry, under the guidance of Professor Raymo, from the University of Miami in 2018. His graduate research involved the design of photoswitchable fluorophores, based on BODIPY

derivatives, and the development of supramolecular delivery strategies for bioimaging applications. He was appointed postdoctoral fellow at Temple University in 2018. His present research interests focus on the development of artificial peptides to replicate the complex molecular recognition and catalytic functions of proteins. He has authored 20 publications in the general areas of fluorescence imaging, materials science, molecular switches and photochemistry.



Ek Raj Thapaliya received a M.Sc. in chemistry from Tribhuvan University (Nepal) in 2006 and a Ph.D., under the guidance of Professor Raymo, from the University of Miami in 2017. His graduate research involved the synthesis and analysis of photoactivatable fluorophores and fluorescent amphiphilic polymers designed for bioimaging applications. He was appointed postdoctoral fellow at the Icahn School of Medicine of Mount Sinai in New York in 2017. His present research interests focus on the synthesis of photocaged compounds for optoneurobiology. He authored 22 publications in the general areas of fluorescence imaging, materials science, molecular switches and photochemistry.



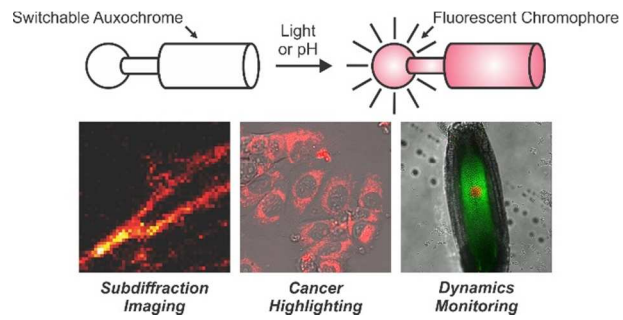
Lorenzo Sansalone received a Laurea Magistrale in Medicinal Chemistry and Pharmaceutical Technologies from the University of Milan (Italy) in 2013 and a Ph.D., under the guidance of Professor

Raymo, from University of Miami in 2018. His graduate research involved the synthesis and analysis of photoactivatable fluorophores for bioimaging applications and photocaged drugs. He was appointed postdoctoral fellow at the Icahn School of Medicine of Mount Sinai in New York in 2018. He authored 4 publications in the general areas of fluorescence imaging, materials science, molecular switches and photochemistry.



Françisco M. Raymo received a Laurea in Chemistry from the University of Messina (Italy) in 1992 and a Ph.D. in Chemistry from the University of Birmingham (UK) in 1996. He was a postdoctoral associate at the University of Birmingham (UK) in 1996–1997 and at the University of California, Los Angeles in 1997–1999. He was appointed Assistant Professor of Chemistry at the University of Miami in 2000 and promoted to Associate Professor in 2004 and Full Professor in 2009. His research interests combine the design, synthesis and analysis of switchable molecular constructs for imaging applications. He authored more than 250 publications.

## Table of Contents



Activatable fluorophores allow the spatiotemporal control of fluorescence required to acquire subdiffraction images, highlight cancer cells and monitor dynamic events